Stem Cell Reports
Resource
OPEN ACCESS

High-Throughput Screening for Modulators of *CFTR* Activity Based on Genetically Engineered Cystic Fibrosis Disease-Specific iPSCs

Sylvia Merkert,[1,2,3,9] Madline Schubert,[1,2,3,9] Ruth Olmer,[1,2,3,9] Lena Engels,[1,2,3] Silke Radetzki,[4] Mieke Veltman,[5,6] Bob J. Scholte,[5,6] Janina Zöllner,[1,2,3] Nicoletta Pedemonte,[7] Luis J.V. Galietta,[8] Jens P. von Kries,[4] and Ulrich Martin[1,2,3,*]

[1]Leibniz Research Laboratories for Biotechnology and Artificial Organs (LEBAO), Department of Cardiothoracic, Transplantation and Vascular Surgery, Hannover Medical School, 30625 Hannover, Germany
[2]REBIRTH-Cluster of Excellence, Hannover Medical School, 30625 Hannover, Germany
[3]Biomedical Research in Endstage and Obstructive Lung Disease (BREATH), Member of the German Center for Lung Research (DZL), 30625 Hannover, Germany
[4]Leibniz-Forschnungsinstitut für Molekulare Pharmakologie (FMP), 13125 Berlin, Germany
[5]ErasmusMC, Sophia Children's Hospital, Pediatric Pulmonology, 3015 AA Rotterdam, The Netherlands
[6]Cell Biology Department Rotterdam, 3015 AA Rotterdam, The Netherlands
[7]UOC Genetica Medica, IRCCS Istituto Giannina Gaslini, 16147 Genova, Italy
[8]Telethon Institute of Genetics and Medicine (TIGEM), 80078 Pozzuoli, Italy
[9]Co-first author
*Correspondence: martin.ulrich@mh-hannover.de
https://doi.org/10.1016/j.stemcr.2019.04.014

SUMMARY

Organotypic culture systems from disease-specific induced pluripotent stem cells (iPSCs) exhibit obvious advantages compared with immortalized cell lines and primary cell cultures, but implementation of iPSC-based high-throughput (HT) assays is still technically challenging. Here, we demonstrate the development and conduction of an organotypic HT Cl^-/I^- exchange assay using cystic fibrosis (CF) disease-specific iPSCs. The introduction of a halide-sensitive *YFP* variant enabled automated quantitative measurement of Cystic Fibrosis Transmembrane Conductance Regulator (*CFTR*) function in iPSC-derived intestinal epithelia. *CFTR* function was partially rescued by treatment with VX-770 and VX-809, and seamless gene correction of the p.Phe508del mutation resulted in full restoration of *CFTR* function. The identification of a series of validated primary hits that improve the function of p.Phe508del *CFTR* from a library of ~42,500 chemical compounds demonstrates that the advantages of complex iPSC-derived culture systems for disease modeling can also be utilized for drug screening in a true HT format.

INTRODUCTION

Patient-specific induced pluripotent stem cells (iPSCs) are considered a valuable tool to model various types of diseases, in particular based on genetic defects. Moreover, it is presumed that iPSC technology, in combination with targeted gene editing technologies, will open a new era in drug development and testing (Ebert et al., 2012; Merkert and Martin, 2018). The development of high-throughput (HT) assays for drug screening, however, is considerably exacerbated by the need for much larger cell numbers, robust differentiation protocols, and the requirement for automated and reliable readout systems. It is therefore not surprising that as yet not many successful iPSC-based screens have been conducted in drug development in a true HT format (Shi et al., 2017).

Despite these apparent challenges, such screens have important advantages compared with primary cells and immortalized cell lines. These include (1) the possibility of collecting patient-specific source cells, (2) the unlimited potential for propagation, (3) the option to generate different cell lineages from one patient-derived cell source, (4) the possibility for targeted genome engineering on a clonal level, (5) the existence of a cell lineage-specific normal intracellular signal cascade, regulation, and proteostasis environment, and (6) the possibility to integrate the influence of genetic modifiers that play an important role in the clinical manifestation of a disease. Overall, it is expected that iPSC-based phenotypic screening approaches will result in higher success rates of compounds than from conventional target-based screens (Vincent et al., 2015).

In the case of cystic fibrosis (CF), recent HT screens have identified modulators of the Cystic Fibrosis Transmembrane Conductance Regulator (*CFTR*), a chloride channel expressed in secretory epithelia (Galietta, 2013). These can be classified as *CFTR* potentiators, which restore the channel activity by enhancing gating, and correctors, which are able to rescue trafficking of specific mutants to the cell surface *in vitro*, including the most common *CFTR* mutant (p.Phe508del). By applying immortalized cell lines, the *CFTR* potentiator VX-770 and the *CFTR* correctors VX-661 and VX-809 were identified. VX-770 was reported to increase chloride secretion about 10-fold in primary human bronchial epithelial (HBE) cells heterozygous for the gating mutation p.Gly551Asp (Van Goor et al.,

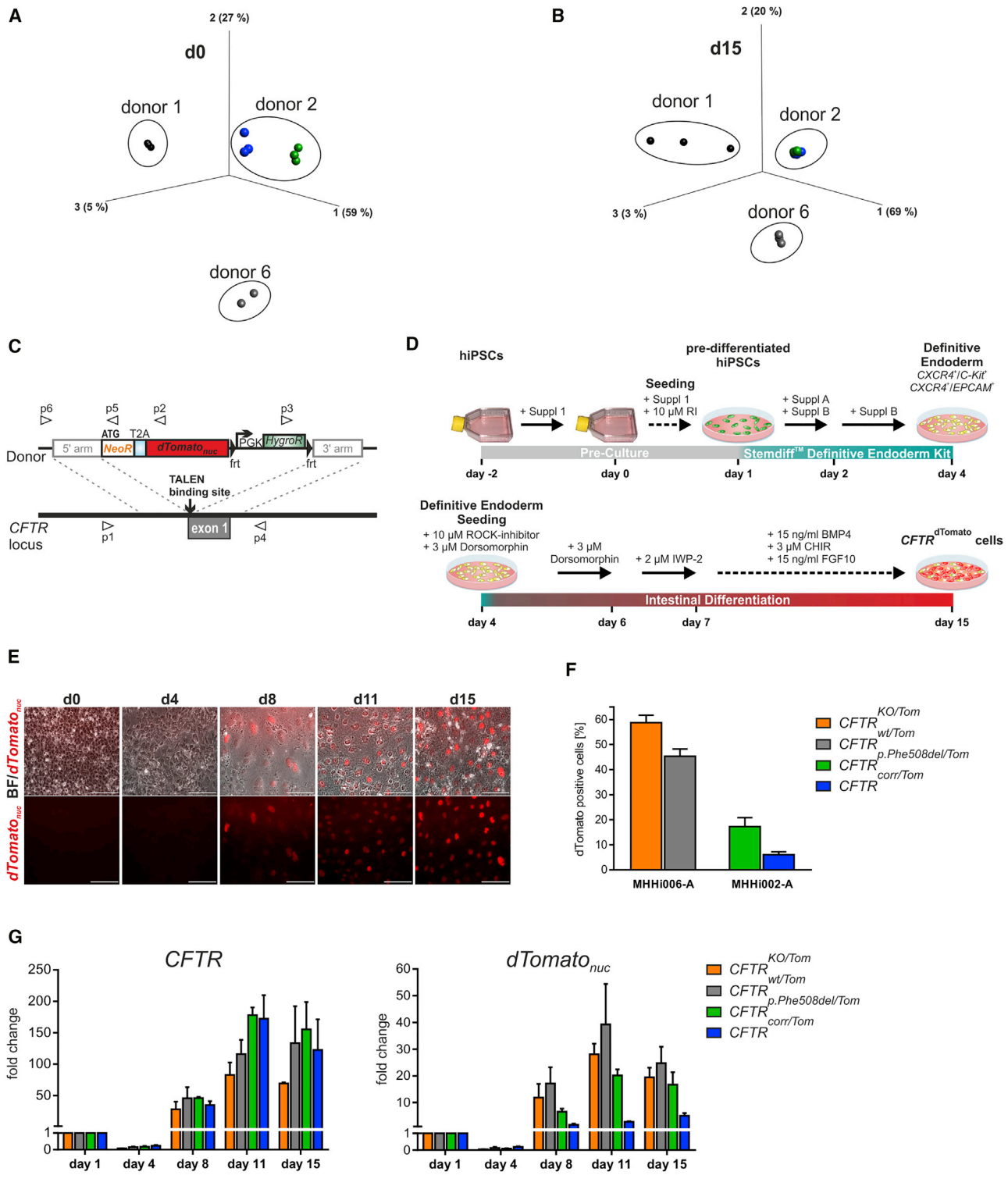

Figure 1. Generation of *CFTR*^{dTomato} Reporter iPSCs and Differentiation into Intestinal Epithelia

(A and B) PCA analysis. Global comparison of different hiPSC lines (healthy donor 1 [MHHi001-A, non-edited, shown in black], donor 2 [MHHi002-A-derived cell lines; CF parental line shown in green and seamless corrected line shown in blue], healthy donor 6 [MHHi006-A-derived line, genetically edited, shown in gray]) by PCA show a clear clustering of the two isogenic lines based on donor 2 and more

(legend continued on next page)

2009), whereby VX-809 was able to enhance chloride secretion in HBE cells from homozygous p.Phe508del patients to 14% of wild-type activity *in vitro* (Van Goor et al., 2011). Results from clinical trials of VX-809 on homozygous patients, however, were modest at best (Clancy et al., 2012). Even with the combination of the potentiator VX-770 and the corrector VX-809 for homozygous p.Phe508del, CF patients showed an improvement in lung function to a relatively low extent (Graeber et al., 2018; Wainwright et al., 2015). The new triple combination of *CFTR* modulators (VX-661, VX-659, VX-770) so far promises considerably more effect (Davies et al., 2018) but needs further evaluation.

It is therefore clear that previous *in vitro* models for correctors are poor predictors of clinical efficacy, although the most promising compounds were even validated on primary human epithelial cells. This underlines the need for the identification of novel compounds with a screening system that closely recapitulates the *in vivo* situation and the complexity of CF disease more accurately and reliable. With patient-derived iPSCs, a suitable source of expandable CF patient-derived cells is now available that can be genetically engineered to establish appropriate reporter cell lines and can be differentiated toward different *CFTR*-expressing derivatives of the most affected organs, including lung (Huang et al., 2015), bile duct (Dianat et al., 2014), and intestinal epithelia (McCracken et al., 2011).

Here, we show that intestinal epithelia differentiated from genetically engineered CF patient-derived iPSCs and their isogenic control cells after seamless correction of the p.Phe508del mutation can be utilized in an HT drug screening approach. Screening of ~42,500 chemical compounds resulted in the identification of a number of validated primary hits that showed rescue of *CFTR* function to a different extent, underlining that even complex functional organotypic screens based on disease-specific iPSC derivatives can be conducted in a true HT format. Further comprehensive analyses are now required to investigate the degree of *CFTR* rescue in primary airway cells to identify binding sites and to elucidate mechanisms of action of the individual compounds.

RESULTS

Requirement for an Isogeneic Control Cell Line with Seamless Correction of the p.Phe508del Mutation

Isogenic iPSC control lines with seamless correction of the respective disease-specific mutation are generally considered as ultimate control in iPSC-based disease modeling. Gene editing of iPSCs and the subsequent clonal selection procedure, however, may not only lead to introduction of new mutations but also to the selection of cell clones with (epi)genetic aberrations that show altered culture characteristics and differentiation behavior. In order to confirm the similarity of the *CFTR* p.Phe508del line MHHi002-A and its seamless corrected counterpart MHHi002-A-1 (Merkert et al., 2017) to be used in our screen, we have compared the global gene expression of both cell lines before and after intestinal differentiation (Figure 1). Principal component analysis (PCA) revealed close clustering of the *CFTR* p.Phe508del line (donor 2 derived) with its isogenic gene-corrected counterpart, but more divergence from two unrelated human iPSC lines (donor 1 and donor 6 derived), either in the undifferentiated state (Figure 1A) or after intestinal differentiation (Figure 1B). This indicates, that despite gene editing and the single-cell cloning procedure, the seamless corrected subclone is still much more similar to the parental cell line than other unrelated iPSC lines, all generated in the same laboratory. This was confirmed by a more detailed comparison of differentially expressed genes (DEGs) between the

divergence from the two other hiPSC lines (donor 1 and donor 6), both in the undifferentiated state on day 0 (A) and on day 15 of directed differentiation (B). n = 3 independent differentiations for each line. For further analyses, also see Figure S1.

(C) Schematic illustration of the targeting strategy applied for TALEN-mediated integration of the neomycin-2A-dTomato$_{nuc}$ reporter cassette. The *CFTR* gene is targeted at exon 1 in-frame with the ATG start codon. Gray arrows indicate primers used to confirm targeted integration of the reporter construct. *NeoR*, neomycin resistance gene; T2A, self-cleaving peptide sequence; *dTomato$_{nuc}$*, dimeric variant of dsRed fluorescent protein coupled to nuclear membrane location signal; frt, flippase recognition target site; PGK, phosphoglycerate kinase promoter; *HygroR*, hygromycin resistance gene.

(D) Schematic illustration of the protocol for iPSC differentiation toward *CFTR^{dTomato}*-expressing intestinal epithelial cells. iPSCs cultured as monolayer were induced to DE via the STEMdiff Definitive Endoderm Kit. Following the application of dorsomorphin and IWP-2, the intestinal specification was promoted using BMP4, CHIR, and FGF10.

(E) Representative fluorescence microscopy showing emerging *dTomato$_{nuc}$*-positive cells during the time course of directed differentiation of *CFTR$^{KO/Tom}$* cells toward epithelial cells. BF, bright field. Scale bars represent 100 μm.

(F) Quantification of *dTomato$_{nuc}$*-positive cells on day 15 of directed differentiation of four *CFTR*-dTomato$_{nuc}$ reporter iPSC lines toward intestinal epithelial cells (mean ± SEM from three independent differentiations).

(G) Fold change of *dTomato$_{nuc}$* and *CFTR* expression during the time course of directed differentiation of four *CFTR*-dTomato$_{nuc}$ reporter iPSC lines (mean ± SEM from three independent differentiations). The knockout allele in the *CFTR$^{KO/Tom}$* line was generated via deletion of the Kozak sequence, which will result in mRNA transcription but not in *CFTR* protein translation (see also Figure S1E).

Table 1. Overview of Generated Reporter iPSC Lines

Name	Parental Line	*CFTR* Genotype[a]	*CFTR* Phenotype	Abbreviation
MHHi006-A-1 (CFTRdTomato74)[b]	MHHi006-A	wild type	functional	$CFTR^{wt/Tom}$
MHHi006-A-3 (CFTRKO/CFTRdTomato89)[b,c]	MHHi006-A	knockout	no protein	$CFTR^{KO/Tom}$
MHHi002-A-3 (CFTRdTomato4)[d]	MHHi002-A	p.Phe508del	mutated	$CFTR^{p.Phe508del/Tom}$
MHHi002-A-2 (CFTRdTomato2)[d,e]	MHHi002-A-1	corrected p.Phe508del	functional	$CFTR^{corr/Tom}$

All cell lines are targeted monoallelic with the $dTomato_{nuc}$ reporter in the *CFTR* locus.
[a]Genotype of the non-targeted *CFTR* allele.
[b]Zeocin-$dTomato_{nuc}$ reporter.
[c]Missing Kozak sequence (initiates translation process) upstream of the ATG start codon of one *CFTR* allele results in monoallelic *CFTR* knockout (for details see Figure S1E).
[d]Neomycin-$dTomato_{nuc}$ reporter.
[e]Based on MHHi002-A, which was heterozygously corrected with ssODNs (Merkert et al., 2017).

applied cell lines, which resulted in higher numbers of DEGs for the comparison of unrelated cell lines, either genetically engineered (donor 6 derived) or not further engineered (donor 1), in contrast to the comparison of the mutation-corrected subclone and its parental cell line (Figures S1A and S1B).

Generation of Human $CFTR^{dTomato}$ Reporter iPSC Lines

Efficiency and reliability of differentiation protocols are a critical prerequisite for application of iPSC-derived cells on an industrial scale, including HT drug screens. In order to enable straightforward monitoring of *CFTR*-expressing cells on a single-cell level during the differentiation of iPSCs, we placed a *dTomato*-fluorescent protein coupled to a nuclear membrane localization signal ($dTomato_{nuc}$) under the control of the *CFTR* locus of a CF_p.Phe508del iPSC line (MHHi002-A) and its heterozygously corrected counterpart (MHHi002-A-1) (Figures 1C, S1C, and S1D). Allele-specific PCR analysis confirmed $dTomato_{nuc}$ integration into the p.Phe508del mutated allele of the heterozygously corrected CF iPSC line (data not shown). For all further procedures and analyses, one correctly targeted clone each was selected from the CF iPSCs and the mutation-corrected iPSCs. In addition, two previously established *CFTR* wild type and knockout control cell lines carrying a *zeocin*™ resistance instead of the *neomycin*™ resistance were applied. For clarity, all selected reporter cell lines that were applied for analysis hereafter are abbreviated according to their *CFTR* genotype: $CFTR^{wt/Tom}$, $CFTR^{KO/Tom}$, $CFTR^{p.Phe508del/Tom}$, and $CFTR^{corr/Tom}$ as listed in Table 1.

Differentiation of $CFTR^{dTomato}$ Reporter iPSC Lines

Considering the very complex, costly, and time-consuming culture protocols for differentiation into airway cells, we decided to develop an HT assay based on *CFTR*-expressing intestinal epithelia, which can be generated using a much shorter and less costly protocol. For the generation of *CFTR*-expressing intestinal epithelia, a stepwise differentiation protocol via definitive endoderm (DE) and posterior endoderm was developed (Figure 1D, for details see Supplemental Information). All cell lines were capable of generating DE as shown by *CXCR4/C-KIT* and *CXCR4/EPCAM* co-staining on day 4 of differentiation (Figures S1F and S1G), although with slightly less efficiency in the case of the $CFTR^{p.Phe508del/Tom}$ and $CFTR^{corr/Tom}$ cell lines. *CFTR*-$dTomato_{nuc}$-positive cells emerged around day 8 during the time course of differentiation. After 15 days, the cultures showed distinct *CFTR*-$dTomato_{nuc}$-expressing cells with clear fluorescence localization restricted to the cell nuclei (Figure 1E). Microscopic quantification of the $dTomato_{nuc}$ signal on day 15 of differentiation resulted in an average of 58% and 45% positive cells for the $CFTR^{KO/Tom}$ and $CFTR^{wt/Tom}$ cell clones and 17% and 6% for the $CFTR^{p.Phe508del/Tom}$ and $CFTR^{corr/Tom}$ clone, respectively (Figure 1F). $dTomato_{nuc}$ mRNA expression started to increase from day 8 of differentiation, which reflected the kinetics of the *CFTR* mRNA expression (Figure 1G) and the appearance of the red fluorescence in the differentiation cultures.

Detailed Characterization of the Intestinal Epithelial Cell Population

Microarray expression analysis of the resulting cell populations on day 15 of differentiation and tissue controls (intestine and liver) were conducted. PCA revealed a clear separation of differentiated (d15) hiPSCs from their undifferentiated (d0) counterparts and adult liver but close clustering with adult intestine (Figure 2A). More detailed comparative expression analyses were conducted for all genes with >2-fold elevated expression ($p > 0.01$) in differentiated (d15) versus undifferentiated iPSCs (d0) and in intestine versus undifferentiated (d0) iPSCs (Table S3). In

total, 4,045 genes were significantly upregulated in the d15 differentiation samples compared with undifferentiated (d0) iPSC samples; 5,018 genes were detected with significantly elevated expression in adult intestinal tissue with its diverse cellular components compared with d0 cells (Table S3). Comparative analysis of both gene lists resulted in an intersection of 2,094 genes (Table S3), which were significantly upregulated in both groups, accounting for about 51% of the upregulated genes in the differentiated cells (Figure 2B). Detailed analysis of the genes with elevated expression showed enrichment of GO terms connected to intestinal absorption (GO 0098865, 0030299), immunity (GO 0002446, 0043312), brush border membrane (GO 0031526), and epithelial cell differentiation (GO0030855) (Figure S2A) (Chen et al., 2013; Kuleshov et al., 2016). Furthermore, differentiated cells and intestine showed a shared expression pattern indicated by the expression levels of selected individual genes involved in digestive tract development, intestinal cell differentiation/development, and genes expressed in the mature intestine (e.g., *SI*, *VIL1*, *LCT*, *ALPI*) (Figure 2C). Markers connected to the development such as *GATA5*, *GATA6*, *CCBR*, *FGFR3*, and *EGFR* were also elevated in the differentiated population, suggesting that the iPSC-derived intestinal cells did not adopt a fully mature adult phenotype. In addition, a gene list (Table S4) compiled of GO term lists connected to intestine development and function as well as gene lists from the human protein atlas for intestine and colon (https://www.proteinatlas.org) was used to further compare expression profiles of undifferentiated cells (d0), differentiated cells (d15), and intestine. The generated heatmap of upregulated genes underlines the intestinal-like expression pattern of the differentiated cells (Figure 2D).

Differentiated *CFTR*-expressing epithelial cells were dissociated on day 15 of differentiation and seeded at high density on membrane inserts for functional analyses. When re-seeding the cells on Laminin-511-coated inserts, low cuboidal morphology and also *ZO-1* expression, indicating intact tight junctions, could be observed (Figure S2B), which consistently (n = 3) resulted in higher transepithelial electrical resistance (TEER) than collagen I/fibronectin or Geltrex coating (data not shown). Four days after seeding, TEER reached on average 1,130 Ω cm^2 in *CFTR* corrected cells and 1,070 Ω cm^2 in the mutated cells (Figure S2C). Apical surface liquid (ASL) height measurements were performed to assess the transepithelial fluid transport capacity of the differentiated cells on the filters. While no response to Forskolin could be observed in *CFTR* mutated cells (Figure S2D), the addition of Forskolin increased the *CFTR*-dependent fluid transport activity in corrected cells at a rate of approximately 12 μm/h, indicating that the iPSC-derived cell population expresses all required apical and basolateral transport systems in addition to the apical chloride channel *CFTR*.

Generation of Halide-Sensitive *eYFP* Reporter iPSC Lines and Measurement of *CFTR* Channel Activity in iPSC-Derived Intestinal Epithelia in a Cl^-/I^- Exchange Assay

For the development of an iPSC-based automatable functional screening approach, a halide-sensitive *eYFP* (HS-*eYFP*) reporter (Figures 3A and 3B) was integrated into the *AAVS1* locus (Figures 3C and S3A) of the four $CFTR^{dTomato}$ iPSC lines listed in Table 1, enabling functional analysis of the endogenous *CFTR* channel. All established reporter iPSC lines exhibited a bright HS-*eYFP* fluorescence signal and retained the hallmarks of pluripotent stem cells, and stable transgene expression was observed in cell types of all three germ layers (Figures 3D, S3B, and S3C).

The four established $AAVS1^{eYFP}/CFTR^{dTomato}$ iPS reporter cell lines were differentiated toward *CFTR*-$dTomato_{nuc}$-expressing intestinal epithelial cells. After 15 days, the cultures developed distinct $dTomato_{nuc}$-positive cells with clear fluorescence localization at the cell nuclei and co-expression of HS-*eYFP* (Figure 3E). The differentiated cells were analyzed for *CFTR* activity in a microscopic Cl^-/I^- exchange assay (Galietta et al., 2001b) (Figure 3F). In the preparation of a plate reader-based HT screening with our differentiated reporter cells, we included a 24 h pre-incubation step for putative correctors in DMSO (Figure 3F). The whole-cell batch analysis of the HS-*eYFP* intensity changes revealed comparable results with the analysis of individual $dTomato_{nuc}$-positive cells (Figure S3D). Therefore, we continued analyzing the HS-*eYFP* fluorescence changes as batch analyses of the entire differentiated cell population. Forskolin stimulation of $CFTR^{wt/Tom}$ and $CFTR^{corr/Tom}$ cells resulted in a significant reduction of the HS-*eYFP* fluorescence after the addition of iodide, which was absent in $CFTR^{KO/Tom}$ as well as in $CFTR^{p.Phe508del/Tom}$ cells (Figure 3G, left graph). To verify the specificity of the *CFTR*-mediated HS-*eYFP* reduction, the *CFTR* channel was specifically inhibited via CFTR(inh)-172, a thiazolidinone-class inhibitor acting as closed-channel stabilizer. CFTR(inh)-172 has been used as a selective inhibitor to identify *CFTR* currents in various cell types (Ma et al., 2002a; Thiagarajah et al., 2004). This resulted in a considerable reduction of halide transport in $CFTR^{wt/Tom}$ and $CFTR^{corr/Tom}$ cells in comparison with Forskolin stimulation only (Figure 3G, right graph). All recorded traces were summarized via calculation of the maximal slope after iodide addition and statistically analyzed (Figure 3H). We obtained significant differences for *CFTR* activation with and without CFTR(inh)-172 treatment in differentiated $CFTR^{wt/Tom}$ as well as in $CFTR^{corr/Tom}$ cells. Furthermore, a significant difference in halide transport was detected between differentiated

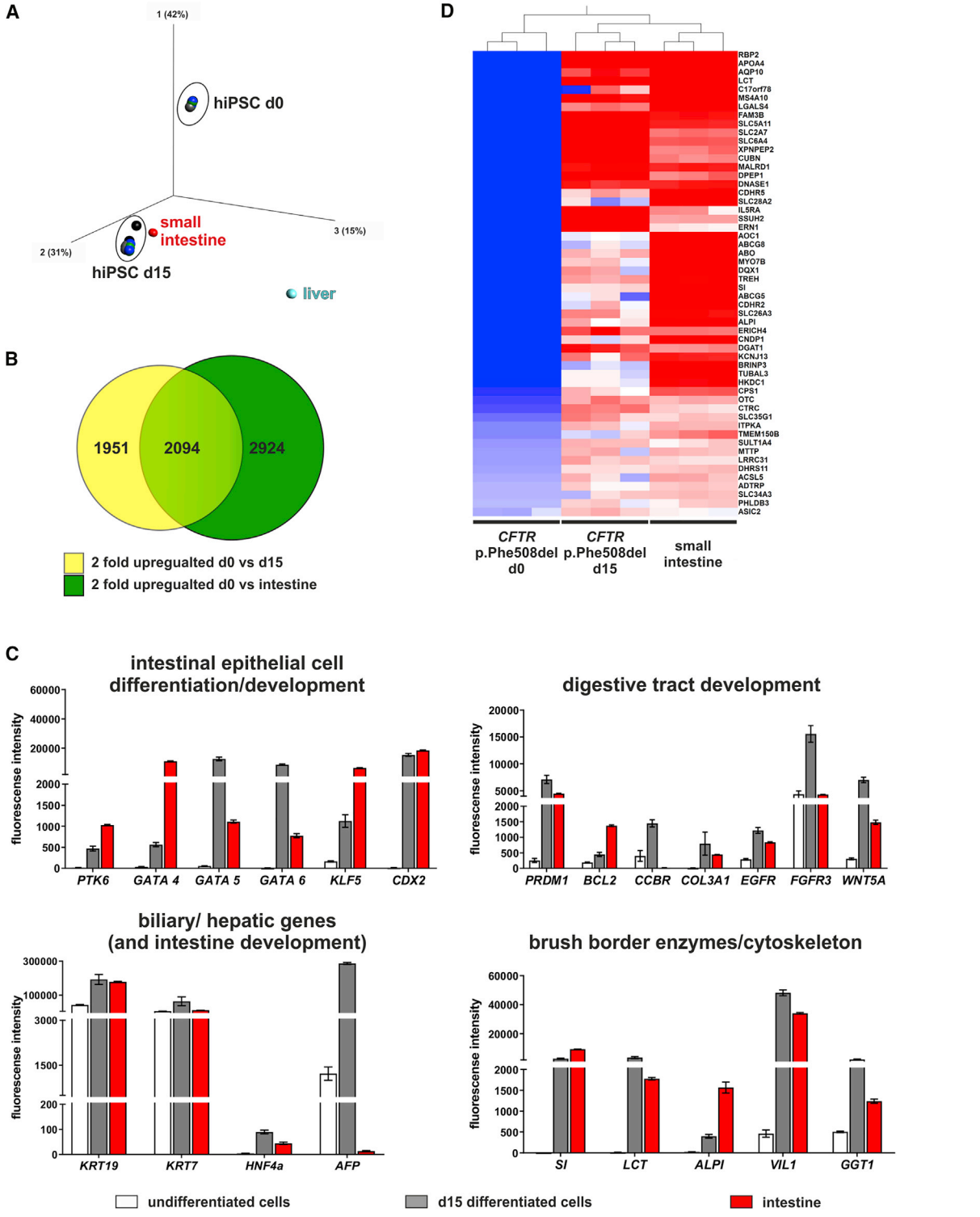

Figure 2. Human iPSC-Derived Epithelial Cells Share Expression Patterns with Adult Intestine

(A) PCA was conducted on undifferentiated hiPSCs (d0) (n = 11, independent biological samples), differentiated hiPSC (d15) (n = 12, independent biological samples), adult intestine (n = 3, technical replicates), and adult liver (n = 3, technical replicates). Differentiated hiPSCs (d15) cluster with adult intestine (in red) but are distinct from undifferentiated hiPSCs (d0) and adult liver (in cyan).

(legend continued on next page)

mutant *CFTR*$^{p.Phe508del/Tom}$ cells and the differentiated gene-corrected *CFTR*$^{corr/Tom}$ cells. Forskolin stimulation of undifferentiated reporter iPSCs and DMSO vehicle control of differentiated reporter iPSCs did not lead to any reduction of the HS-*eYFP* signal after addition of iodide (Figures S3E and S3F).

Development and Conduction of an HT Screening Assay

In order to use our functional iPSC-based assay for HT drug screening, the iPSC-derived *CFTR*-expressing intestinal epithelial cells were dissociated on day 13 of differentiation and re-plated into a 384-well format using a device microplate dispenser. A seeding density of 10,000 cells/well was chosen to ensure the formation of a tight epithelial layer. The re-plated cells re-adhered, spread, and formed tight junctions as demonstrated on day 15 of differentiation, the time point of the Cl^-/I^- exchange assay, via immunofluorescence staining. The tight junction marker protein *ZO-1* and the expression of fetal intestinal markers such as *AFP*, *CDX2*, and *SOX9* could be confirmed, as well as the co-expression of the HS-*eYFP* (Figure S4A).

The HS-*eYFP* fluorescence changes of *CFTR*$^{corr/Tom}$ and *CFTR*$^{p.Phe508del/Tom}$ cells were acquired using a fully automated fluorescent image plate reader (FLIPR^{TM}) and revealed a significant reduction of the HS-*eYFP* signal in the gene-corrected *CFTR*$^{corr/Tom}$ cells, which was absent in the mutant *CFTR*$^{p.Phe508del/Tom}$ cells (Figures 4A and 4B). We further evaluated the effect of the approved *CFTR* corrector VX-809 to rescue the halide transport in differentiated mutant *CFTR* cells in combination with the potentiator VX-770 and two other correctors, VX-661 and corr-4a (Pedemonte et al., 2005). VX-809 and/or VX-661 or corr-4a were added 24 h prior to Forskolin activation at different concentrations at lower temperature of 28°C (Pedemonte et al., 2005; Van Goor et al., 2011). VX-770 was added always at a constant concentration of 1 μM in parallel to Forskolin. Treatment of cells with 0.2 μM and 10 μM VX-809 at 28°C led to significantly reduced HS-*eYFP* fluorescence compared with the control (Figure 4B). The combination of VX-809 and VX-661 showed no further improvement of the *CFTR* function compared with VX-809 alone. An additive effect could be observed for the combination of VX-809 and corr-4a, which resulted in the highest p.Phe508del activity (Figures 4A and 4B).

We performed a primary HT screen of ~42,500 compounds from the FMP compound library of the chemical biology platform (Lisurek et al., 2010) at a single concentration of 10 μM. The whole screening workflow (Figure 4C) comprising cell seeding on day 13 of differentiation, medium exchange, and compound transfer on day 14, as well as the Cl^-/I^- exchange assay on day 15, was performed in an automated manner. This enabled the handling of up to 26 384-well plates per differentiation batch leading to the accomplishment of the whole library after five screening rounds. The quality of the differentiated cell batches was assessed by day 4 flow cytometry analyses for DE formation and day 13 qPCR analysis for *CFTR* and *CDX2* expression (Figures S4B and S4C). We calculated the slopes from the FLIPR^{TM} kinetic curves using R software and evaluated the performance of our assay based on the range between positive (corrected cells) and negative controls (mutated cells). We assessed the assay quality using in-house software, applying Z' factor and Z score calculations for each screening plate. Generated graphics enabled visualization of the statistical value distribution over plate and edge effects (Figure 4D). The Z' factor, which represents the assay response window, was 0.55, supporting the feasibility and reproducibility of the screening (Figure 4E). Potential hits were identified by determination of the relative activity of the compounds in comparison with the mutated (value 0) and the genetically corrected cells (value 1). After fixation and staining of cell nuclei, automated image analysis for determination of cell numbers/well was applied to detect the potential toxicity of individual compounds (Figure 4F). After primary screening, we identified 86 hit compounds with a relative activity >0.38 (Figure 5A). For these compounds, a validation run was performed, whereby 11 concentrations from 20 μM to 0.02 μM were tested in duplicates. All 86 tested compounds were ranked according to their relative activity compared with the hit cutoff of 0.38 as well as by visual confirmation of the kinetic curves. This resulted in preselection of 21 verified hits (Figure 5B). Among those, seven compounds reached the relative

(B) A Venn diagram was created from gene lists containing genes with ≥2-fold elevated expression ($p > 0.01$) in d15 differentiation cultures compared with d0 cultures (yellow, 4,045 genes) and in adult intestine compared with d0 cultures (green, 5,018 genes). The intersection of both gene lists contains 2,094 genes.

(C) Relative expression levels of selected individual genes connected to intestinal epithelial cell differentiation/development, digestive tract development, biliary/hepatic cells (and also intestinal development), as well as brush border enzymes/cytoskeleton in undifferentiated iPSCs (d0; n = 11), differentiated iPSCs (d15; n = 12), and adult intestine (n = 3).

(D) A heatmap of upregulated genes in differentiated cells (d15) and intestine compared with undifferentiated cells (d0) was created based on a gene list compiled of GO terms connected to intestine development and function (http://www.geneontology.org/) and genes listed in the human protein atlas for intestine and colon (https://www.proteinatlas.org/), further demonstrating that differentiated cells are more similar to adult intestine than to undifferentiated cells (d0).

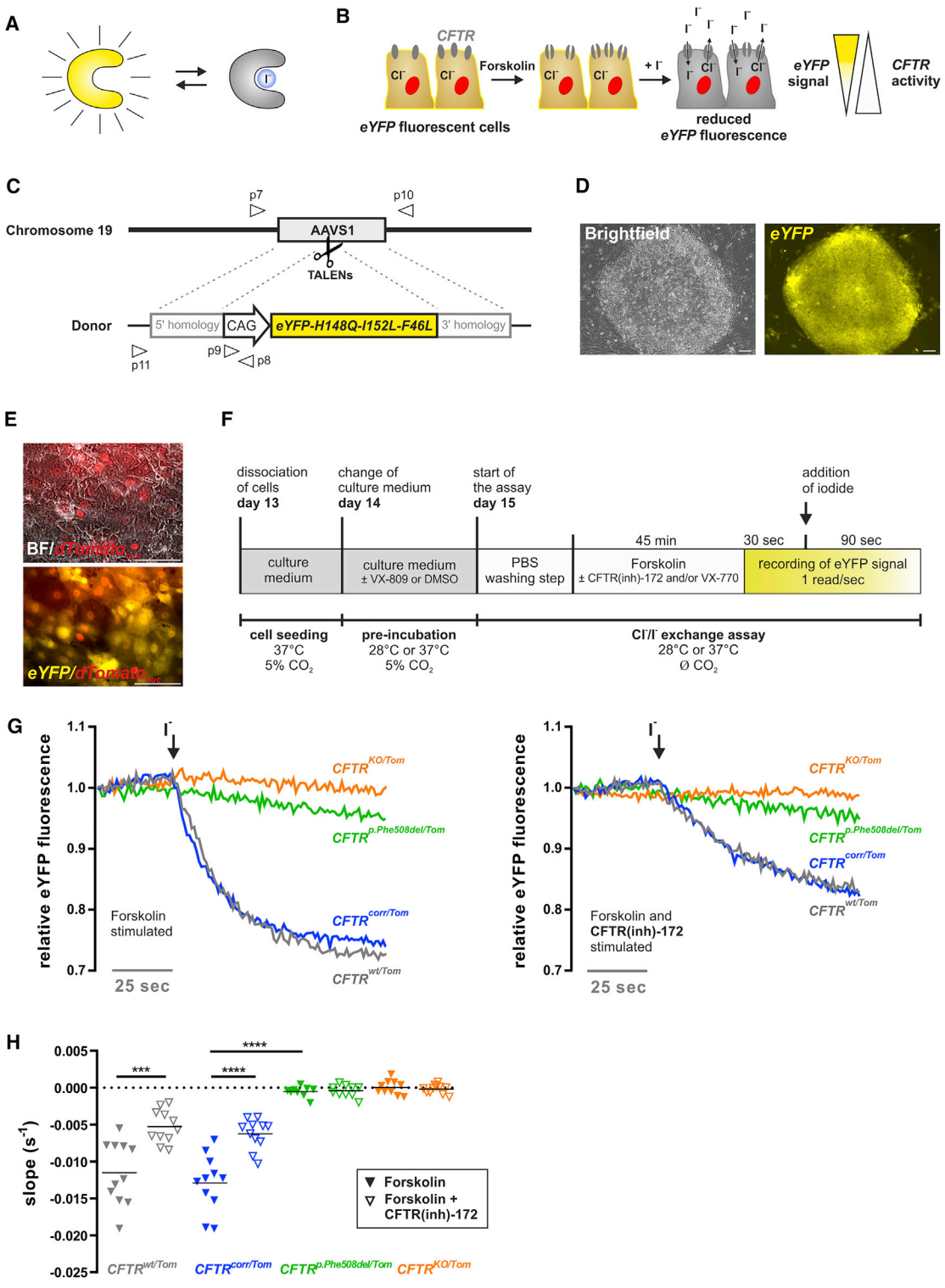

Figure 3. Generation of Human Halide-Sensitive *AAVS1*^{eYFP}/*CFTR*^{dTomato} Reporter iPSC Lines that Express Functional *CFTR* after Directed Differentiation into Intestinal Epithelia

(A) Binding of iodide to the HS-*eYFP* protein results in a reduced fluorescence intensity.

(B) Simplified schematic representation of the chloride/iodide exchange assay to analyze *CFTR* function. *CFTR* channel stimulation via Forskolin allows iodide influx into the cell leading to decreased HS-*eYFP* fluorescence intensity.

(legend continued on next page)

activity hit cutoff at a concentration of 10 μM, nine compounds at 20 μM, and five compounds were included as borderline compounds although they showed less activity at both concentrations (Figures 5C, S5A, and S5B). Among those 21, we selected our ten most promising compounds (Figures S5C and S5D) as the top candidates for prioritized testing for chemical structure clustering as well as further investigation in secondary assays.

DISCUSSION

To capture the pathophysiology of a disease, the application of organotypic iPSC-based models that incorporate the genomic background in connection with the corresponding clinical phenotypes already in the earliest *in vitro* assays may result in better clinical translation (Engle and Vincent, 2014; Swinney and Anthony, 2011). Since genetic modifiers play an important role in the clinical manifestation of CF (Tümmler and Stanke, 2014), we did not consider unrelated wild-type iPSCs as proper control for the patient-derived $CFTR^{p.Phe508del/Tom}$ cells, but applied isogenic corrected cells generated by targeted gene editing for the HT screen. While it has been shown that the genetic background contributes to the CF phenotype, it has not been investigated in detail whether mutations and epigenetic differences unintentionally acquired during targeted gene editing or selected during the single-cell cloning procedure may also cause functional alterations relevant for disease modeling and drug screening. We therefore considered it important to explore the degree of similarity between the two cell lines used in the HT screen, the $CFTR^{p.Phe508del/Tom}$ iPSC line and the disease corrected counterpart $CFTR^{corr/Tom}$, including their differentiated progeny. Remarkably, our microarray analysis underlines the general significance of isogenic control cell lines. Despite various steps of genetic engineering and single-cell cloning, both undifferentiated and differentiated derivatives of the seamless corrected subclone (applied as positive control in our HT screen) cluster much closer to their mutated parental counterparts in terms of DEGs than two unrelated *CFTR* wild-type iPSC lines with different genetic background.

Since robust and reliable differentiation protocols are a basic requirement for iPSC-based HT screens, we sought to eliminate sources of interference wherever possible. In order to achieve a robust intestinal differentiation, we always started from iPSC monolayers cultured under defined conditions. Moreover, a commercial endoderm differentiation kit, which in our hands yielded the most reproducible results, and, as far as possible, small molecules instead of recombinant proteins were applied to further increase the reliability of the differentiation protocol. During subsequent differentiation, intestinal marker genes, including *CDX2*, *SI*, and *VIL1*, were significantly upregulated. In addition, we also found upregulation of genes frequently considered as hepatic and biliary genes (e.g., *AFP*, *HNF4a*, *KRT19*, *KRT7*). This might be prevented by addition of FGF4, which was shown to suppress the formation of hepatic gene expression at the hindgut stage (Tamminen et al., 2015). The hepatic and biliary markers detected, however, are also known to be expressed on intestinal cells during development (Cirillo et al., 1995; Stammberger and Baczako, 1999; Tsai et al., 2017; Verzi et al., 2013). Since on the other hand some marker genes for mature secretory epithelia cells (e.g., *MUC2*, *CHGA*) are not expressed in our intestinal cell population, we conclude that our intestinal cell population does not show a fully mature adult phenotype.

The use of iPSC lines that express a $dTomato_{nuc}$ fluorochrome under control of one allele of the *CFTR* locus enabled visualization of *CFTR*-expressing cells during intestinal differentiation. Because of the lack of reliable anti *CFTR* antibodies for the detection of relatively low physiological protein expression levels (Kalin et al., 1999; Mendes et al., 2004), we refrained from co-staining of our $dTomato_{nuc}$-expressing cells with any *CFTR* antibodies.

(C) Schematic illustration of the *AAVS1* targeting strategy. The donor vector contains an *eYFP-H148Q-I*152L-*F46*L expression cassette flanked by two arms of *AAVS1* locus homology sequences. Gray arrows represent primers used for PCR analysis to confirm targeted integration of the reporter construct. CAG, cytomegalovirus early enhancer element coupled to chicken β-actin promoter; *eYFP-H148Q-I152-F46*L, halide-sensitive enhanced yellow fluorescent protein.

(D) Microscopic images of a transgenic $AAVS1^{eYFP}$ iPSC clone on feeder cells. Scale bars represent 100 μm.

(E) Representative live imaging of $AAVS1^{eYFP}/CFTR^{dTomato}$ reporter cells on day 15 of directed differentiation. Scale bars represent 100 μm.

(F) Timeline of cell seeding, cell preparation, and chloride/iodide exchange assay. If required, cells were pre-incubated for 24 h with VX-809 or vehicle containing culture medium 1 day after re-seeding. For the HS-*eYFP* assay, cells were incubated with 20 μM Forskolin ± 20 μM CFTR(inh)-172 ± 1 μM VX-770. Subsequently, HS-*eYFP* fluorescence was microscopically recorded for 120 s, whereby 137 mM sodium iodide was added after 30 s.

(G) Representative traces of HS-*eYFP* fluorescence changes for all four reporter cell lines on day 15 of directed differentiation. Arrows indicate iodide addition. Cells were either stimulated with 20 μM Forskolin (left) or with 20 μM CFTR(inh)-172 + 20 μM Forskolin (right) prior to addition of iodide.

(H) Statistical analysis of the maximal slopes of the fluorescence changes obtained from microscopic HS-*eYFP* assay for all four reporter cell lines (n = 9–11 traces from at least three independent differentiations; black lines show the mean).

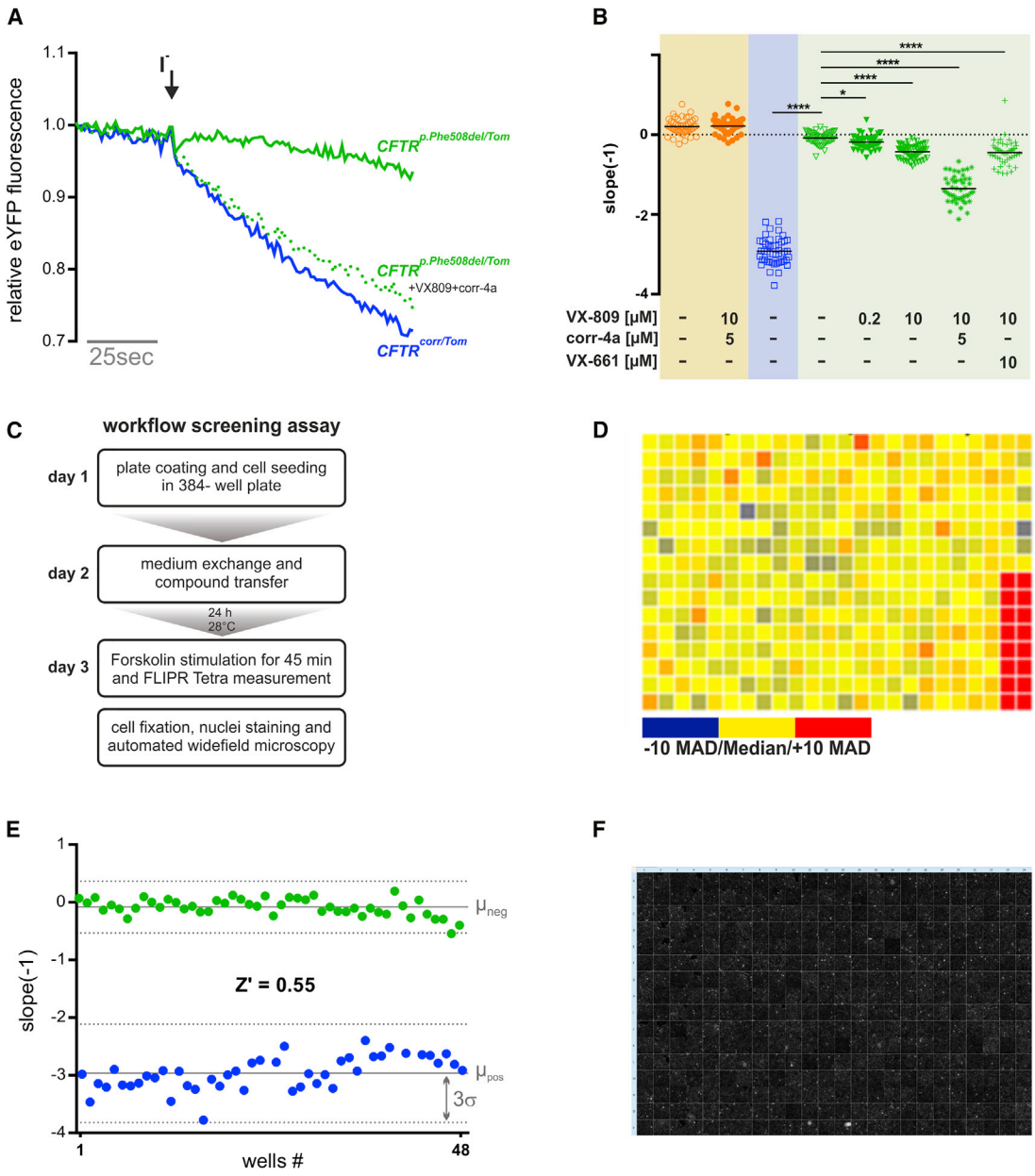

Figure 4. Development of an Automated Assay for High-Throughput Measurement of *CFTR* Function in iPSC-Derived Epithelial Cells

(A) Representative FLIPR^{TM} HS-*eYFP* fluorescence kinetic data of differentiated *CFTR*$^{corr/Tom}$ cells (blue) and *CFTR*$^{p.Phe508del/Tom}$ cells (green) in 384-well format. Arrow indicates iodide addition. Dotted line represents *CFTR*$^{p.Phe508del/Tom}$ cells pre-incubated with 10 µM VX-809 and 5 µM corr-4a for 24 h. All wells were pre-incubated at 28°C and treated with 1 µM VX-770 (each trace represents three wells).

(B) Statistical analysis of the slopes from the FLIPR^{TM} kinetic curves, after 24 h CFTR rescue, via treatment with VX-809, corr-4a, or VX-661, as indicated. Cells were incubated at 28°C, stimulated with 20 µM Forskolin, and in all experiments the potentiator VX-770 was applied at 1 µM (n = 48 wells; black lines show the mean). *CFTR*$^{KO/Tom}$ cells are depicted in orange, *CFTR*$^{corr/Tom}$ cells are depicted in blue, *CFTR*$^{p.Phe508del/Tom}$ cells are depicted in green.

(C) Schematic workflow of the 3-day screening procedure, starting from day 13 of differentiation with the plating of the cells in 384-well format until automated HS-*eYFP* assay at day 15 of differentiation.

(D) Heatmap of a representative screening plate, displaying the median of the statistic value as gradient color (−10 MAD, median, +10 MAD). The last two columns contain the control samples. MAD, median absolute deviation.

(E) The calculation of the *Z'* factor demonstrates the signal window of the HT assay. $Z'_{standard}$ value calculation was performed based on the maximal slope from the FLIPR kinetic curves. The plot represents representative data of 48 replicate wells across a 384-well plate of both

(legend continued on next page)

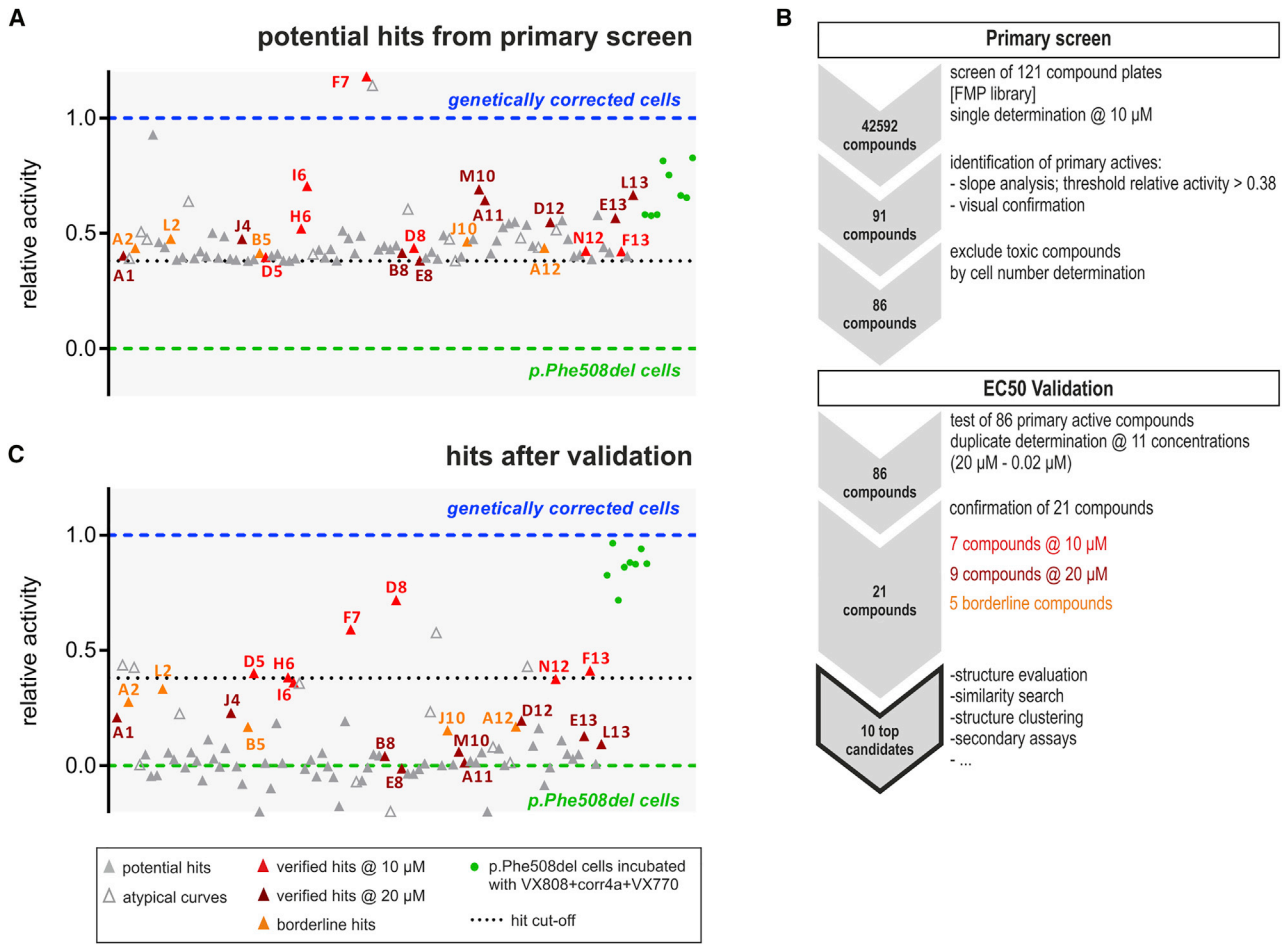

Figure 5. High-Throughput Screening of the FMP Library Identifies Chemical Modulators of *CFTR* Function

(A) Scatterplot graph of potential hits from the primary screen at 10 µM. Depicted are all compounds (triangles) resulting in relative activity >0.38 (dotted line), which are considered hits. The library was distributed over 121 384-well plates; each plate contains 8 positive control wells (represented by a blue line), 8 negative control wells (represented by a green line), 8 control wells with p.Phe805del cells incubated with VX-809 and corr-4a (exemplarily shown as green dots), and 8 CFTR knockout wells (data not shown). All plates were incubated for 24 h at 28°C; 1 µM VX-770 was added for 45 min before HS-*eYFP* assay performance.

(B) Overview of screening steps with filters for compound selection.

(C) Scatterplot graph of EC_{50} validation at 10 µM as the mean (n = 2 independent plates). Depicted are all 86 potential hits from the primary screen. Compounds confirming relative activity above hit cutoff at 10 µM are depicted in red, at 20 µM in dark red, and borderline compounds in orange.

Nevertheless, since the kinetics of *CFTR*-dTomato$_{nuc}$ mRNA expression correspond to the appearance of *dTomato$_{nuc}$*-positive cells during differentiation, and because the *CFTR* mRNA expression detected could be functionally confirmed in our HS-*eYFP* assay, there is no reason to doubt the specificity of the *dTomato$_{nuc}$* reporter, which is placed under control of the endogenous *CFTR* locus.

It is noteworthy that both reporter lines derived from MHHi006-A reproducibly showed a substantially higher proportion of *CFTR*-dTomato$_{nuc}$-expressing cells than the MHHi002-A derived lines. In addition, we observed

negative (mutated cells in green) and positive (genetically corrected cells in blue) controls. Three data points were determined as outliers and subsequently removed from the positive replicate data. Gray solid lines represent the mean (µ), dotted lines represent respective 3-fold SD (σ).

(F) Cell distribution of a representative 384-well screening plate monitored by automated microscopy of Hoechst 33342 stained nuclei. Counted nuclei analysis was used for exclusion of toxic compounds.

differences in terms of the formation of *CFTR*-dTomato$_{nuc}$-expressing cells also between the genetically engineered subclones of MHHi006-A, and between subclones of MHHi002-A. Already the efficiency of endoderm differentiation was line dependent with both MHHi006-A lines reproducibly yielding about 90% pure DE under the given conditions. These differences were accompanied by clear differences in the proliferation rates of the four lines during culture expansion and further differentiation. The differing proliferation rates of the four lines very likely explain at least in part the different amounts of *CFTR*-positive cells, and may be adjustable by individualized timing of the differentiation protocol for each line. The observed different proliferation and differentiation characteristics underline the impact of the genetic background and clonal variations.

In addition to the availability of functional iPSC derivatives that allow mimicking the disease in a dish, another critical requirement for iPSC-based HT screens is the potential for automation. For measurement of *CFTR* function *in vitro*, in particular the use of a halide-sensitive eYFP reporter, is straightforward and can be automated due to its simplicity and sensitivity (Ma et al., 2002b). The respective HS-*eYFP* (Galietta et al., 2001a), however, has so far been applied only for functional measurement of *CFTR* transgenes overexpressed in immortalized cell lines (Ma et al., 2002b; Park et al., 2016) but not to analyze more moderate levels of endogenous *CFTR* in primary epithelia or stem cell derivatives. Here, we demonstrate that the halide-sensitive *eYFP-H148Q-I*152L-*F46*L variant facilitates measurement of endogenous *CFTR* function in iPSC-derived epithelia. While a normal *CFTR* response was detected in *CFTR*$^{wt/Tom}$ cells, no significant decrease in the HS-*eYFP* fluorescence could be observed in the *CFTR*$^{KO/Tom}$ cells.

Remarkably, the seamless correction of the *CFTR* p.Phe508del mutation in the *CFTR*$^{corr/Tom}$ cell line perfectly restored *CFTR* function to wild-type levels in our microscope-based HS-*eYFP* assay as well as in the plate reader setting. Furthermore, the *CFTR* function detected in *CFTR*$^{wt/Tom}$ and *CFTR*$^{corr/Tom}$ cells could be blocked by CFTR(inh)-172. Similar to other studies in which *CFTR* overexpressing cell lines were applied (Caci et al., 2008; Fischer et al., 2010; Ma et al., 2002a), we did not observe full inhibition of the *CFTR* channel activity, which might be an effect of the interior negative membrane potential of epithelial cells reducing the CFTR(inh)-172 potency. Interestingly, we observed comparable levels of *CFTR* function in intestinal epithelia derived from the MHHi006-A CFTR wild type and the genetically corrected MHHi002-A-1 iPSC line, although the proportion of *CFTR*-dTomato$_{nuc}$-expressing cells in the respective differentiation cultures was quite divergent (6% versus 45%; see also discussion above). Actually, probably two effects may contribute to this phenomenon: (1) dTomato^{pos} cells within the cell population represent those cells that show high levels of *CFTR* expression, while other cells that do not show a detectable dTomato expression may express lower but still substantial levels of *CFTR*, and (2) *CFTR*-dTomato^{pos} and *CFTR*-dTomato^{neg} cells couple via gap junctions that propagate the halide influx to neighboring cells (Bjerknes et al., 1985; Gumber et al., 2014).

As proof of concept for the usefulness of our iPSC-based assay in drug development, we analyzed the approved *CFTR* drug combination Orkambi (*CFTR* corrector VX-809 and *CFTR* potentiator VX-770) to rescue the *CFTR* p.Phe508del in iPSC-derived intestinal epithelia. Pre-incubation of *CFTR*$^{p.Phe508del/Tom}$ with VX-809 and VX-770 at 28°C led to 5-fold increased *CFTR* function, demonstrated by HS-*eYFP* decrease. The additional application of corr-4a even increased the *CFTR* function up to 17-fold. This represents almost 50% *CFTR* function compared with the gene-corrected control. Comparable studies applying the HS-*eYFP* assay with *CFTR* p.Phe508del overexpressing immortalized cell lines, reached up to 25% *CFTR* function after pre-incubation with VX-809 at 37°C (Favia et al., 2014; Vijftigschild et al., 2013). Also the application of VX-809 and VX-770 in p.Phe508del human bronchial epithelial cells resulted in a *CFTR*-mediated chloride transport that reached levels equivalent to approximately 25% of that measured in non-CF HBE (Van Goor et al., 2011). Although 28°C pre-incubation does not reflect physiological conditions, we chose 28°C pre-incubation to increase the likelihood for the identification of even weak *CFTR* correctors (Pedemonte et al., 2005), which might be useful for drug combination strategies and still bear the potential for improvement after structural optimization.

Finally, we adapted our assay to the 384-well HT plate reader format and conducted an HT screen for potential *CFTR* modulators in a fully automated screening environment. Intestinal epithelia cells instead of airway cells were chosen for the HT assay because of the shorter, more reproducible, and less cost-intensive differentiation protocol. Further validation of compounds and testing of compound combinations can be performed in secondary assays on different disease-relevant cell types derived from the same CF reporter iPSC lines, as well as on primary airway cells or intestinal organoids from other patients.

In conclusion, our study underlines the feasibility of HT screens based on iPSC-derived epithelia for identification of potentiators and correctors of mutated *CFTR*. Clonal genome engineering approaches can be utilized in iPSCs to integrate fluorescence reporters that enable visualization of *CFTR* expression during differentiation and facilitate automated measurement of *CFTR* function at an HT scale. In contrast to p.Phe508del *CFTR* overexpressing immortalized cell lines, iPSC-based screens incorporate the influence

of the proteostasis environment on CF disease and the efficacy of correctors. Our approach, based on cells with a more physiological array of proteins involved in protein folding, quality control, degradation, and trafficking, and with more physiological levels of *CFTR* expression, will favor the development of correctors with novel mechanisms of action, more relevant to the therapeutic goal *in vivo*. Forthcoming HT screens will show whether such iPSC-based organotypic assays are better predictors of clinical compound efficacy than conventional HT screens.

EXPERIMENTAL PROCEDURES

For detailed description see Supplemental Experimental Procedures.

Cell Culture

We used the HSC_F1285_T-iPS2 (Hartung et al., 2013) cell line, registered (https://hpscreg.eu/) as MHHi006-A, the CF iPSC line MHHi002-A and its corrected counterpart MHHi002-A-1 (Merkert et al., 2017), all generated in our research group. Unless indicated otherwise, all pluripotent stem cell lines were cultured under standard conditions essentially as previously described (Merkert et al., 2014).

TALEN-Based Targeted Gene Editing

For the integration of the reporter constructs, iPSCs grown as monolayer cultures were dissociated and transfected with the respective TALEN expression and donor plasmids. Cells were seeded either onto hygromycin-resistant feeder cells for *CFTR* targeting or on Geltrex coated culture vessels for *AAVS1* targeting. For the generation of $CFTR^{dTomato}$ reporter cell lines, the hygromycin-based clone selection was initiated 72 h post transfection for 4 days. Arising colonies were transferred manually onto irradiated feeder cells to generate single-cell clones. For the generation of $AAVS1^{eYFP}$ reporter cell lines, $eYFP^{pos}$ cells were sorted via fluorescence-activated cell sorting and plated in limiting dilution. Upcoming colonies were picked manually and expanded clonally.

iPSC Differentiation

In a stepwise differentiation protocol, iPSCs from monolayers in essential 8 (E8) medium were first differentiated to DE via a STEMdiff Definitive Endoderm Kit (TeSR-E8 Optimized) from STEMCELL Technologies. DE cells on day 4 of differentiation were cultured for 2 days in the presence of dorsomorphin and ROCK inhibitor. Thereafter, cells were treated for 1 day with IWP-2. From day 7 until day 15, cells were cultured in the presence of CHIR99021, BMP4, and FGF10.

Microscope-Based Chloride/Iodide Exchange Assay

Cells on day 13 of differentiation and undifferentiated cells serving as controls were seeded on glass-bottom dishes (Figure 3F). On day 15, individual cell or batch analysis of *eYFP* fluorescence intensity after addition of sodium iodide was performed microscopically at 37°C. Cells were washed once with PBS and incubated with Forskolin, Forskolin + CFTR(inh)-172, or respective DMSO control, respectively. *eYFP* fluorescence was recorded continuously for 120 s with one picture per second. Thirty seconds after the start of recording, iodide-rich PBS was added and the fluorescence intensity was measured for another 90 s. Negative values reflect a decrease of *eYFP* fluorescence intensity.

Plate Reader-Based Chloride/Iodide Exchange Assay

Cells were dissociated on day 13 of differentiation and seeded on black 384-well plates. The next day, the compounds were applied in differentiation medium and incubated for 24 h at 28°C. To start the assay, the cells were washed three times with PBS and incubated for 45–50 min at room temperature with 20 μM Forskolin + 1 μM VX-770. The *eYFP* fluorescence intensity was analyzed for 120 s with 1 read/s in an FLIPR Tetra system. After 30 s, the 2.75-fold volume of iodide-rich PBS was automatically added, and the change in *eYFP* fluorescence intensity further monitored. Afterward, the cells were fixed with paraformaldehyde and stained with Hoechst 33342 for automated cell counting.

Statistics

Statistical analyses were performed with GraphPad Prism6 and the results are presented as means ± SEM, unless otherwise noted. Significance of two groups was analyzed using the unpaired t test. Statistical significance was assigned as follows: *$p \leq 0.05$; **$p \leq 0.01$; ***$p \leq 0.001$; ****$p \leq 0.0001$.

SUPPLEMENTAL INFORMATION

Supplemental Information can be found online at https://doi.org/10.1016/j.stemcr.2019.04.014.

AUTHOR CONTRIBUTIONS

S.M., M.S., and U.M designed the study; S.M., M.S., J.Z., and S.R. performed the experiments; S.M., M.S., R.O., and U.M. analyzed and interpreted the data; L.E. generated *CFTR* reporter lines MHHi006-A-1 and MHHi006-A-3; M.V. and B.J.S. performed TEER analysis, confocal microscopy, ASL measurements, analyzed and interpreted data, and evaluated the manuscript; L.J.V.G. provided HS-*eYFP*; N.P., L.J.V.G., J.P.v.K. gave conceptual advice; S.M., M.S., R.O., and U.M. wrote the paper.

ACKNOWLEDGMENTS

The authors thank J. Beier, T. Kohrn, and A. Otto for providing technical assistance, as well as R. Diestel for data management support. We are thankful to B. Tümmler and M. Amaral for helpful discussions, to T. Scheper for providing bFGF, A. Kirschning and G. Dräger for providing CHIR99021 and Y-27632. We thank the Cell-Sorting Core Facility of Hannover Medical School for cell sorting, the Confocal Laser Microscopy Core Facility of Hannover Medical School for their introduction into confocal microscopy, and the RUCG Transcriptomics of Hannover Medical School for performing the microarrays. The authors thank C. Seyffarth and R. Leu, Leibniz Institute for Molecular Pharmacology, Berlin, for technical assistance for the conduction of the screening, as well as Medicinal Chemistry (M. Nazaré) at the FMP, Berlin, for compound management. We also thank G.J. Kremers for developing the automated microscope stage protocol and ImageJ algorithm used to analyze the Z scans in ASL measurements. This work was

funded by the German Center for Lung Research (DZL; 82DZL002A1), German Research Foundation, Cluster of Excellence REBIRTH (EXC 62/1, EXC 62/3), Mukoviszidose Institut GmbH (1404), and ERA-Net for Research Programs on Rare Diseases (01GM1601).

Received: November 22, 2017
Revised: April 10, 2019
Accepted: April 11, 2019
Published: May 9, 2019

REFERENCES

Bjerknes, M., Cheng, H., and Erlandsen, S. (1985). Functional gap junctions in mouse small intestinal crypts. Anat. Rec. *212*, 364–367.

Caci, E., Caputo, A., Hinzpeter, A., Arous, N., Fanen, P., Sonawane, N., Verkman, A.S., Ravazzolo, R., Zegarra-Moran, O., and Galietta, L.J. (2008). Evidence for direct CFTR inhibition by CFTR(inh)-172 based on Arg347 mutagenesis. Biochem. J. *413*, 135–142.

Chen, E.Y., Tan, C.M., Kou, Y., Duan, Q., Wang, Z., Meirelles, G.V., Clark, N.R., and Ma'ayan, A. (2013). Enrichr: interactive and collaborative HTML5 gene list enrichment analysis tool. BMC Bioinformatics *14*, 128.

Cirillo, L.A., Emerson, J.A., Vacher, J., and Tyner, A.L. (1995). Developmental regulation of alpha-fetoprotein expression in intestinal epithelial cells of transgenic mice. Dev. Biol. *168*, 395–405.

Clancy, J.P., Rowe, S.M., Accurso, F.J., Aitken, M.L., Amin, R.S., Ashlock, M.A., Ballmann, M., Boyle, M.P., Bronsveld, I., Campbell, P.W., et al. (2012). Results of a phase IIa study of VX-809, an investigational CFTR corrector compound, in subjects with cystic fibrosis homozygous for the F508del-CFTR mutation. Thorax *67*, 12–18.

Davies, J.C., Moskowitz, S.M., Brown, C., Horsley, A., Mall, M.A., McKone, E.F., Plant, B.J., Prais, D., Ramsey, B.W., Taylor-Cousar, J.L., et al. (2018). VX-659-tezacaftor-ivacaftor in patients with cystic fibrosis and one or two Phe508del alleles. N. Engl. J. Med. *379*, 1599–1611.

Dianat, N., Dubois-Pot-Schneider, H., Steichen, C., Desterke, C., Leclerc, P., Raveux, A., Combettes, L., Weber, A., Corlu, A., and Dubart-Kupperschmitt, A. (2014). Generation of functional cholangiocyte-like cells from human pluripotent stem cells and HepaRG cells. Hepatology *60*, 700–714.

Ebert, A.D., Liang, P., and Wu, J.C. (2012). Induced pluripotent stem cells as a disease modeling and drug screening platform. J. Cardiovasc. Pharmacol. *60*, 408–416.

Engle, S.J., and Vincent, F. (2014). Small molecule screening in human induced pluripotent stem cell-derived terminal cell types. J. Biol. Chem. *289*, 4562–4570.

Favia, M., Mancini, M.T., Bezzerri, V., Guerra, L., Laselva, O., Abbattiscianni, A.C., Debellis, L., Reshkin, S.J., Gambari, R., Cabrini, G., et al. (2014). Trimethylangelicin promotes the functional rescue of mutant F508del CFTR protein in cystic fibrosis airway cells. Am. J. Physiol. Lung Cell. Mol. Physiol. *307*, L48–L61.

Fischer, H., Illek, B., Sachs, L., Finkbeiner, W.E., and Widdicombe, J.H. (2010). CFTR and calcium-activated chloride channels in primary cultures of human airway gland cells of serous or mucous phenotype. Am. J. Physiol. Lung Cell. Mol. Physiol. *299*, L585–L594.

Galietta, L.J. (2013). Managing the underlying cause of cystic fibrosis: a future role for potentiators and correctors. Paediatr. Drugs *15*, 393–402.

Galietta, L.J., Haggie, P.M., and Verkman, A.S. (2001a). Green fluorescent protein-based halide indicators with improved chloride and iodide affinities. FEBS Lett. *499*, 220–224.

Galietta, L.V., Jayaraman, S., and Verkman, A.S. (2001b). Cell-based assay for high-throughput quantitative screening of CFTR chloride transport agonists. Am. J. Physiol. Cell Physiol. *281*, C1734–C1742.

Graeber, S.Y., Dopfer, C., Naehrlich, L., Gyulumyan, L., Scheuermann, H., Hirtz, S., Wege, S., Mairbaurl, H., Dorda, M., Hyde, R., et al. (2018). Effects of lumacaftor-ivacaftor therapy on cystic fibrosis transmembrane conductance regulator function in Phe508del homozygous patients with cystic fibrosis. Am. J. Respir. Crit. Care Med. *197*, 1433–1442.

Gumber, S., Nusrat, A., and Villinger, F. (2014). Immunohistological characterization of intercellular junction proteins in rhesus macaque intestine. Exp. Toxicol. Pathol. *66*, 437–444.

Hartung, S., Schwanke, K., Haase, A., David, R., Franz, W.M., Martin, U., and Zweigerdt, R. (2013). Directing cardiomyogenic differentiation of human pluripotent stem cells by plasmid-based transient overexpression of cardiac transcription factors. Stem Cells Dev. *22*, 1112–1125.

Huang, S.X., Green, M.D., de Carvalho, A.T., Mumau, M., Chen, Y.W., D'Souza, S.L., and Snoeck, H.W. (2015). The in vitro generation of lung and airway progenitor cells from human pluripotent stem cells. Nat. Protoc. *10*, 413–425.

Kalin, N., Claass, A., Sommer, M., Puchelle, E., and Tummler, B. (1999). DeltaF508 CFTR protein expression in tissues from patients with cystic fibrosis. J. Clin. Invest. *103*, 1379–1389.

Kuleshov, M.V., Jones, M.R., Rouillard, A.D., Fernandez, N.F., Duan, Q., Wang, Z., Koplev, S., Jenkins, S.L., Jagodnik, K.M., Lachmann, A., et al. (2016). Enrichr: a comprehensive gene set enrichment analysis web server 2016 update. Nucleic Acids Res. *44*, W90–W97.

Lisurek, M., Rupp, B., Wichard, J., Neuenschwander, M., von Kries, J.P., Frank, R., Rademann, J., and Kuhne, R. (2010). Design of chemical libraries with potentially bioactive molecules applying a maximum common substructure concept. Mol. Divers. *14*, 401–408.

Ma, T., Thiagarajah, J.R., Yang, H., Sonawane, N.D., Folli, C., Galietta, L.J., and Verkman, A.S. (2002a). Thiazolidinone CFTR inhibitor identified by high-throughput screening blocks cholera toxin-induced intestinal fluid secretion. J. Clin. Invest. *110*, 1651–1658.

Ma, T., Vetrivel, L., Yang, H., Pedemonte, N., Zegarra-Moran, O., Galietta, L.J., and Verkman, A.S. (2002b). High-affinity activators of cystic fibrosis transmembrane conductance regulator (CFTR) chloride conductance identified by high-throughput screening. J. Biol. Chem. *277*, 37235–37241.

McCracken, K.W., Howell, J.C., Wells, J.M., and Spence, J.R. (2011). Generating human intestinal tissue from pluripotent stem cells in vitro. Nat. Protoc. *6*, 1920–1928.

Mendes, F., Farinha, C.M., Roxo-Rosa, M., Fanen, P., Edelman, A., Dormer, R., McPherson, M., Davidson, H., Puchelle, E., De Jonge, H., et al. (2004). Antibodies for CFTR studies. J. Cyst. Fibros *3*(Suppl 2), 69–72.

Merkert, M., Bednarski, C., Göhring, G., Cathomen, T., and Martin, U. (2017). Generation of a gene-corrected isogenic control iPSC line from cystic fibrosis-patient specific iPSCs homozygous for p.Phe508del mutation mediated by TALENs and ssODN. Accepted manuscript. Stem Cell Res. *23*, 95–97.

Merkert, S., and Martin, U. (2018). Targeted gene editing in human pluripotent stem cells using site-specific nucleases. Adv. Biochem. Eng. Biotechnol. *163*, 169–186.

Merkert, S., Wunderlich, S., Bednarski, C., Beier, J., Haase, A., Dreyer, A.K., Schwanke, K., Meyer, J., Gohring, G., Cathomen, T., et al. (2014). Efficient designer nuclease-based homologous recombination enables direct PCR screening for footprintless targeted human pluripotent stem cells. Stem Cell Reports *2*, 107–118.

Park, J., Khloya, P., Seo, Y., Kumar, S., Lee, H.K., Jeon, D.K., Jo, S., Sharma, P.K., and Namkung, W. (2016). Potentiation of DeltaF508- and G551D-CFTR-mediated Cl- current by novel hydroxypyrazolines. PLoS One *11*, e0149131.

Pedemonte, N., Lukacs, G.L., Du, K., Caci, E., Zegarra-Moran, O., Galietta, L.J., and Verkman, A.S. (2005). Small-molecule correctors of defective DeltaF508-CFTR cellular processing identified by high-throughput screening. J. Clin. Invest. *115*, 2564–2571.

Shi, Y., Inoue, H., Wu, J.C., and Yamanaka, S. (2017). Induced pluripotent stem cell technology: a decade of progress. Nat. Rev. Drug Discov. *16*, 115–130.

Stammberger, P., and Baczako, K. (1999). Cytokeratin 19 expression in human gastrointestinal mucosa during human prenatal development and in gastrointestinal tumours: relation to cell proliferation. Cell Tissue Res. *298*, 377–381.

Swinney, D.C., and Anthony, J. (2011). How were new medicines discovered? Nat. Rev. Drug Discov. *10*, 507–519.

Tamminen, K., Balboa, D., Toivonen, S., Pakarinen, M.P., Wiener, Z., Alitalo, K., and Otonkoski, T. (2015). Intestinal commitment and maturation of human pluripotent stem cells is independent of exogenous FGF4 and R-spondin1. PLoS One *10*, e0134551.

Thiagarajah, J.R., Song, Y., Haggie, P.M., and Verkman, A.S. (2004). A small molecule CFTR inhibitor produces cystic fibrosis-like submucosal gland fluid secretions in normal airways. FASEB J. *18*, 875–877.

Tsai, Y.H., Nattiv, R., Dedhia, P.H., Nagy, M.S., Chin, A.M., Thomson, M., Klein, O.D., and Spence, J.R. (2017). In vitro patterning of pluripotent stem cell-derived intestine recapitulates in vivo human development. Development *144*, 1045–1055.

Tümmler, B., and Stanke, F. (2014). Genetic and environmental modifiers of cystic fibrosis. In Cystic Fibrosis, M.A. Mall and J.S. Elborn, eds. (European Respiratory Society Monograph), Chapter 4.

Van Goor, F., Hadida, S., Grootenhuis, P.D., Burton, B., Cao, D., Neuberger, T., Turnbull, A., Singh, A., Joubran, J., Hazlewood, A., et al. (2009). Rescue of CF airway epithelial cell function in vitro by a CFTR potentiator, VX-770. Proc. Natl. Acad. Sci. U S A *106*, 18825–18830.

Van Goor, F., Hadida, S., Grootenhuis, P.D., Burton, B., Stack, J.H., Straley, K.S., Decker, C.J., Miller, M., McCartney, J., Olson, E.R., et al. (2011). Correction of the F508del-CFTR protein processing defect in vitro by the investigational drug VX-809. Proc. Natl. Acad. Sci. U S A *108*, 18843–18848.

Verzi, M.P., Shin, H., San Roman, A.K., Liu, X.S., and Shivdasani, R.A. (2013). Intestinal master transcription factor CDX2 controls chromatin access for partner transcription factor binding. Mol. Cell. Biol. *33*, 281–292.

Vijftigschild, L.A., van der Ent, C.K., and Beekman, J.M. (2013). A novel fluorescent sensor for measurement of CFTR function by flow cytometry. Cytometry A *83*, 576–584.

Vincent, F., Loria, P., Pregel, M., Stanton, R., Kitching, L., Nocka, K., Doyonnas, R., Steppan, C., Gilbert, A., Schroeter, T., et al. (2015). Developing predictive assays: the phenotypic screening "rule of 3". Sci. Transl. Med. *7*, 293ps215.

Wainwright, C.E., Elborn, J.S., and Ramsey, B.W. (2015). Lumacaftor-ivacaftor in patients with cystic fibrosis homozygous for Phe508del CFTR. N. Engl. J. Med. *373*, 1783–1784.